

# The *ROSAT* X-ray Background Dipole

M. Plionis & I. Georgantopoulos

*National Observatory of Athens, I. Metaxa & B. Pavlou, Lofos Koufou, Palaia Penteli, 15236, Athens, Greece*

23 October 2018

## ABSTRACT

We estimate the dipole of the diffuse 1.5 keV X-ray background from the *ROSAT* all-sky survey map of Snowden et al (1995). We first subtract the diffuse Galactic emission by fitting to the data an exponential scale height, finite radius, disk model. We further exclude regions of low galactic latitudes, of local X-ray emission (eg the North Polar Spur) and model them using two different methods. We find that the *ROSAT* X-ray background dipole points towards  $(l, b) \approx (288^\circ, 25^\circ) \pm 19^\circ$  in consistency with the Cosmic Microwave Background (within  $\sim 30^\circ$ ); its direction is also in good agreement with the *HEAO-1* X-ray dipole at harder energies. The normalised amplitude of the *ROSAT* XRB dipole is  $\sim 1.7$  per cent. Subtracting from the *ROSAT* map the expected X-ray background dipole due to the reflex motion of the observer with respect to the cosmic rest frame (Compton-Getting effect) we find the large-scale dipole of the X-ray emitting extragalactic sources having an amplitude  $\mathcal{D}_{\text{LSS}} \sim 0.9\mathcal{D}_{\text{XRB}}$ , in general agreement with the predictions of Lahav et al (1997). We finally estimate that the Virgo cluster is responsible for  $\sim 20$  per cent of the total measured XRB dipole amplitude.

**Keywords:** cosmology: cosmic microwave background - large-scale structure of Universe - cosmology: observations - X-rays: general

## 1 INTRODUCTION

According to the paradigm that the X-ray background (XRB) originates mainly from sources at redshifts  $1 < z < 3$  (eg Shanks et al. 1991), it should provide a means of measuring the well established solar motion with respect to the cosmic rest-frame, defined by the Cosmic Microwave Background (CMB), towards  $l = 264^\circ$ ,  $b = 48^\circ$  (cf. Lineweaver et al 1996). An imprint of this reflex motion should be a dipole pointing towards the direction of the CMB dipole (Compton-Getting effect). The available all-sky X-ray maps (*HEAO-1* and *ROSAT*) are composed by X-ray counts not only originating from such distant sources but also from local extragalactic sources ( $z < 0.1$ ). These gravitating extragalactic objects, which cause our peculiar motion with respect to the cosmic rest frame, emit X-rays and therefore their dipole should also point towards the CMB dipole. This has been demonstrated for the case of AGNs (Miyaji & Boldt 1994) and of X-ray clusters (Lahav et al 1989;

Plionis & Kolokotronis 1998). Therefore, the dipole pattern of the XRB results from at least two effects; (a) the motion of the observer with respect to the XRB which in the context of the cosmic-ray background was discussed first by Compton & Getting (1935) and (b) the X-ray emission of extragalactic objects the gravitational field of which causes the observers motion with respect to the cosmic rest frame. The relative contribution of these effects have been analytically estimated by Lahav, Piran & Treyer (1997) and were found to be of the same order of magnitude.

The dipole anisotropy of the XRB has been measured in hard X-rays (2-10 keV) using UHURU (Protheroe, Wolfendale & Wdoczyk 1980) and *HEAO-1* data (Shafer & Fabian 1983, Jahoda 1993). The resulting dipole was found to point towards the general direction of the CMB dipole but with a large uncertainty: the 90 per cent confidence levels quoted by Shafer & Fabian (1983) cover 12 per cent of the whole sky. The use of the *ROSAT* all-sky survey can extend these studies to soft

energies with higher sensitivity and angular resolution. Kneissl et al. (1997) presented a cross-correlation of the COBE DMR and the *ROSAT* all-sky survey maps. However, their attempt to measure the extragalactic dipole was hampered by the contamination of the Galactic emission which is appreciable, especially at low Galactic latitudes, even in the hard *ROSAT* band. They concluded that proper modelling of the Galactic contribution is necessary in order to obtain a measurement of the dipole. In this letter, we attempt to model the diffuse Galactic component using a simple disk model. After subtracting our Galaxy model, we estimate the cosmological X-ray dipole using the *ROSAT* all-sky survey hard maps (1.5 keV) of Snowden et al. (1995).

## 2 THE *ROSAT* ALL-SKY SURVEY DATA

We use the *ROSAT* all-sky survey maps at a mean energy of 1.5 keV (PSPC PI channels 91-201). These maps are now publicly released and are described in detail in Snowden et al. (1995). The maps cover  $\sim 98$  per cent of the sky with a resolution of 2 degrees. Point sources detected in the all-sky survey are included in the maps. The particle background, scattered solar X-ray background and other non-cosmic background contamination components have been removed (see Snowden et al. 1994, Snowden et al. 1995).

The X-ray emission in the 1.5 keV band is mainly extragalactic: Hasinger et al. (1998) have resolved about 70 per cent of the background at these energies into discrete extragalactic sources. However, there is some contamination, due to the poor energy resolution of the *ROSAT* PSPC, from a Galactic component. This is well-fitted with a Raymond-Smith spectrum, having a temperature of  $\sim 0.17$  keV, and may be associated with the Galaxy halo (see Wang & McCray 1993, Gendreau et al. 1995, Hasinger 1996, Pietz et al. 1998). We note that at higher energies (3-60 keV) there is evidence for a even harder Galactic component with a bremsstrahlung spectrum of 9 keV (Iwan et al. 1982); however, this is expected to contribute less than one per cent in the *ROSAT* 1.5 keV band. Moreover, the 1.5 keV maps of Snowden et al. (1995) show some extended features superimposed on the extragalactic and the diffuse hard Galactic component (see Snowden et al. 1995) mainly originating from nearby supernova remnants (eg the North Polar Spur, the Cygnus superbubble). All the above local features must be subtracted before deriving the extragalactic X-ray dipole.

## 2.1 Modelling the Galactic emission

The derivation of a detailed Galactic emission model requires observations in many wavebands and is outside the scope of this paper; detailed modelling of the Galactic halo is discussed in Iwan et al. (1982), Nousek et al. (1982) and Pietz et al. (1998). Here instead, we attempt to make a rough model of the Galactic contamination in our energy band. We model the diffuse Galactic components with a finite radius disk with an exponential scale height, (eg Iwan et al. 1982) which provides a good description of the Galactic component at both soft (0.75 keV) and hard energies (2-60 keV). This is given by:

$$\mathcal{C}(l, b) = C_b \left[ 1 + \frac{Eh}{\sin |b|} \left( 1 - e^{-f(l, R_d) \tan |b|/h} \right) \right] \quad (1)$$

where  $f(l, R_d) = \cos l + \sqrt{R_d^2 - \sin^2 l}$ , with  $\mathcal{C}$  the total X-ray intensity,  $C_b$  the average extragalactic component, in units of  $10^{-6}$  cts  $s^{-1}$   $\text{arcmin}^{-2}$ ,  $E$  the fraction of the total X-ray emission which is due to the Galaxy,  $h$  and  $R_d$  the disk scale height and disk radius, respectively both in units of 10 kpc (the galactocentric distance of the Sun). We exclude from the fit the regions of the most apparent extended emission features: the bulge and the North Polar Spur (ie.  $-40^\circ < b < 75^\circ$  and  $300^\circ \lesssim l \lesssim 30^\circ$  eg Snowden et al. 1997) as well as the Galactic plane strip (with  $|b| < 20^\circ$  or  $30^\circ$ ). Although it is unknown whether there is some small residual bulge emission outside the above excised region, our rough model should provide a good first order approximation to the Galactic halo emission. Furthermore, applying a homogeneous mean count we mask the most apparent "local" extragalactic features; a  $4^\circ$  radius region around the Virgo cluster ( $l, b \approx 287^\circ, 75^\circ$ ) and a  $10^\circ$  radius region around the Magellanic clouds ( $l, b \approx 278^\circ, -32^\circ$ ).

In the minimization procedure we weight each pixel by  $1/\sigma$ , where  $\sigma = (\sigma_I^2 + \sigma_P^2)^{1/2}$ , with  $\sigma_I^2$  the variance of the X-ray *ROSAT* counts due to the intrinsic extragalactic fluctuations and  $\sigma_P^2$  the variance due to Poisson count statistics. We estimate  $\sigma_I$  excluding from the map the North Polar Spur and the  $|b| \leq 45^\circ$  regions and find  $\sigma_I \approx 0.27\mathcal{C}$ . Starting from different initial guesses of the input parameters the minimization procedure does not reach a unique minimum, although the reduced  $\chi^2$  is around one and the output model parameters are closely clustered. This suggests the existence of a broad and shallow minimum. We therefore run 1000  $\chi^2$  minimizations starting from a broad range of initial values. These values are centred on those that Iwan et al (1982) find for the Galactic component using *HEAO-1* data, ie.,  $\langle h \rangle \approx 7$  kpc,  $\langle R_d \rangle \approx 28$  kpc and  $\langle E \rangle \lesssim 10$  per cent; while the input extragalactic contri-

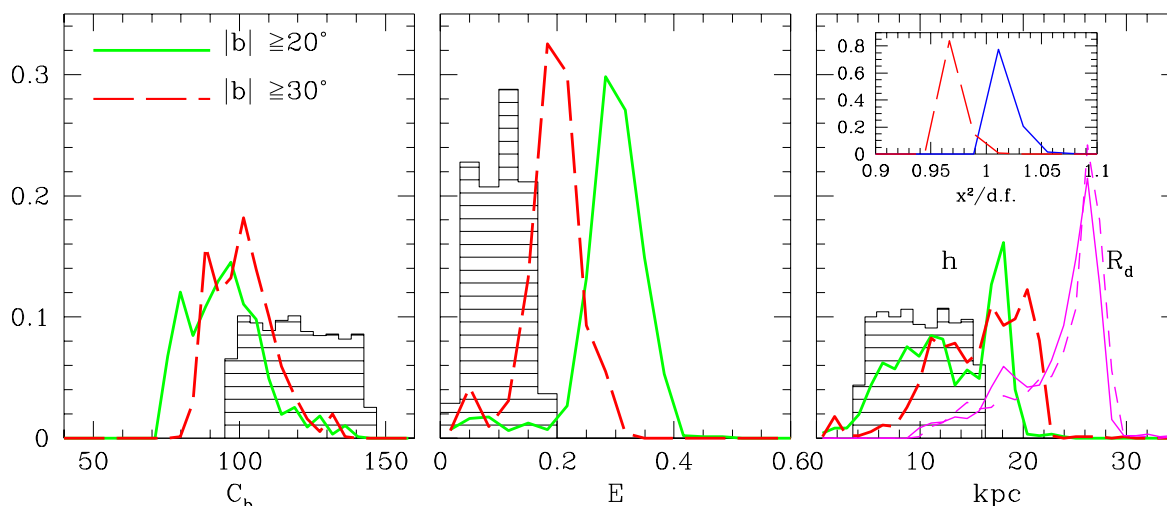


**Figure 1.** Distribution of the finite Galaxy disk model parameters. Continuous lines represent the output parameter distribution while the hatched histograms the corresponding input ones, used to start the  $\chi^2$  minimization procedure.

tribution is centred on  $\langle C_b \rangle \approx 120$ , the value obtained from the *ROSAT* XRB spectral fits in this band (eg Georgantopoulos et al. 1996). The results cluster around some preferred values as can be seen in figure 1, in which we show as hatched histograms the distribution of the input parameters and as thick lines the best-fit output parameter distribution. The most probable values of the fitted parameters as well as their standard deviation over the 1000 minimizations are presented in table 1. For  $|b| > 20^\circ$  we have typically that  $\chi^2 \approx 33600$  for 33064 degrees of freedom and hence this model cannot be rejected. The Galaxy contributes a significant fraction ( $E \sim 20 - 30$  per cent) of the average total *ROSAT* 1.5 keV X-ray emission. As discussed earlier this Galactic component could arise as contamination from lower energies (eg from the 0.17 keV Raymond-Smith Galactic component) due to the coarse energy resolution of the *ROSAT* PSPC. Although this percentage is rather high it is not inconsistent with XRB spectral fits in deep *ROSAT* and *ASCA* pointings: the excellent spectral resolution *ASCA* spectrum of the XRB in the 0.4-10 keV band (Gendreau et al. 1995) presents a steep upturn at 1 keV, suggesting a high contamination of the 1.5 keV *ROSAT* band from lower energy photons. The scale height of the finite emitting disk is  $\sim 16$  kpc, higher than both the value obtained by Pietz et al. (1998) in the 0.75 keV *ROSAT* band and by Iwan et al (1982) in the 2-60 keV *HEAO-1* band. Using the above best-fit model, the predicted Galactic halo luminosity is  $L_x \approx 2 \times 10^{39}$  ergs  $s^{-1}$ . The best-fit extragalactic component arises to  $\sim 100 \pm 11 \times 10^{-6}$  cts  $s^{-1}$  arcmin $^{-2}$ . This value is in excellent agreement with the extrapolation of the *HEAO-1* 3-60 keV data of Marshall et

**Table 1.** Fitted Galaxy model parameters for  $|b| \geq b_{lim}$ .

$b_{lim}$	$C_b$	$E$	$h$ (kpc)	$R_d$ (kpc)
$20^\circ$	$95 \pm 13$	$0.29 \pm 0.06$	$15 \pm 5$	$27 \pm 5$
$30^\circ$	$100 \pm 11$	$0.20 \pm 0.05$	$17 \pm 5$	$27 \pm 5$
$20^\circ$	120 (frozen)	$0.28 \pm 0.10$	$4 \pm 2$	$15 \pm 4$

al. (1980) in the *ROSAT* band but  $\sim 20$  per cent lower ( $\sim 1.5\sigma$ ) than the normalization of the extragalactic power-law component obtained from XRB spectral fits in deep, high galactic latitude *ROSAT* fields (Hasinger 1996). If instead we force the extragalactic contribution to the value obtained from the *ROSAT* XRB fits ( $\sim 120 \times 10^{-6}$  cts  $s^{-1}$  arcmin $^{-2}$  in this band, eg Georgantopoulos et al. 1996) then the best-fit parameters are  $h = 4 \pm 2$  kpc,  $R_d = 15 \pm 4$  kpc and  $E = 0.28 \pm 0.10$  consistent with the values of Pietz et al. (1998). We finally note that, had we not excluded the North Polar Spur region in our fit, with all four parameters ( $C_b, E, h, R_d$ ) free, we would have erroneously obtained a significantly higher Galactic fraction ( $E \sim 40$  per cent) as well as a larger scale height ( $\sim 19$  kpc) but with an unacceptable fit in this case ( $\chi^2_{red} \approx 1.2$ ).

### 3 XRB *ROSAT* DIPOLE

#### 3.1 Dipole fitting procedure

The multipole components of the *ROSAT* X-ray intensity are calculated by summing moments. The dipole moment is estimated by weighing the unit directional vector pointing to each  $40^2$  arcmin $^2$  *ROSAT* cell with the X-ray intensity  $C_i$  of that cell. We normalize the

dipole by the monopole term (the mean X-ray intensity over the sky):

$$\mathcal{D} \equiv \frac{|\mathbf{D}|}{M} = \frac{\sum \mathcal{C}_i \hat{\mathbf{r}}_i}{\sum \mathcal{C}_i} \quad (2)$$

We attempt to estimate the cosmological XRB dipole by applying the above procedure to the *ROSAT* counts after subtracting our best Galaxy model (table 1) and the regions of Galactic and "local" extragalactic X-ray emission. To this end we mask: (a) The Galactic plane, (b) the area dominated by the Galactic bulge and the North Polar Spur (see definitions in section 2.1) and (c) a region of  $10^\circ$  radius around the Large Magellanic Clouds (we have verified that small variations in the limits of all the above regions do not change appreciably our results).

We use two methods to model these regions: the first consists in substituting the observed intensity with the mean value estimated at high galactic latitudes (*homogeneous filling procedure*) and the second based on a *spherical harmonic* extrapolation procedure (cf. Yahil et al 1986). Since the later is slightly more involved we briefly review the method which is based on expanding the sky surface density field  $\sigma(\vartheta, \varphi)$  in real spherical harmonics:

$$\sigma(\vartheta, \varphi) = \sum_{l,m} a_l^m Y_l^m(\vartheta, \varphi) \quad (3)$$

where  $\vartheta = 90^\circ - \text{Gal. latitude}$ ,  $\varphi = \text{Gal. longitude}$  (do not confuse the multipole  $l$  with the Galactic Longitude). In this formulation the normalized dipole is defined as

$$\mathcal{D} = \frac{1}{3a_0^0} \left[ \sum_{m=-1}^1 (a_m^1)^2 \right]^{1/2} \quad (4)$$

where the factor 3 enters for consistency with the definition of eq.2. The observed,  $\Sigma(\vartheta, \varphi)$ , and intrinsic surface density field  $\sigma(\vartheta, \varphi)$ , are related according to:  $\Sigma(\vartheta, \varphi) = \mathcal{M}(\vartheta, \varphi) \sigma(\vartheta, \varphi)$ , where the mask  $\mathcal{M}(\vartheta, \varphi)$  takes values of 1 or 0 depending on whether the  $(\vartheta, \varphi)$  direction points in an observed or excluded part of the sky, respectively. Since we are interested in recovering the dipole ( $l = 1$ ) components of  $\sigma(\vartheta, \varphi)$ , the correction terms should at least involve the quadrupole ( $l = 2$ ) components. Expanding  $\Sigma(\vartheta, \varphi)$  up to the quadrupole order and allowing for the orthogonality relation of the Legendre polynomials, we can express the observed coefficients  $A_l^m$ , in terms of the intrinsic ones,  $a_l^m$ , forming a  $9 \times 9$  matrix, the inversion of which then gives  $a_l^m$ . A more accurate procedure would entail an expansion to higher order  $l$ 's (cf. Lahav et al. 1994) but to recover a smooth underlying dipole structure (in which higher order  $l$ 's are negligible) we have verified, using mock samples, that the above procedure recovers extremely

accurately the direction and amplitude of the true underlying dipole.

### 3.2 Dipole Results

In table 2 we present our main results for different treatment of the data. It is evident that when using the raw *ROSAT* data, the dipole points roughly towards the Galactic centre (in agreement with Kneissl et al 1997). However, when we exclude both the Galaxy and the North Polar Spur, the measured dipole is in much better directional agreement with the CMB dipole. For the *homogeneous filling* method we find  $\delta\theta_{cmb} < 20^\circ$  excluding the Galactic plane below  $|b| = 20^\circ$  or  $|b| = 30^\circ$ . For the *spherical harmonic* method the misalignment angle is larger,  $\delta\theta_{cmb} > 39^\circ$ . The Virgo cluster, being quite near and very bright in X-rays, could contribute significantly to the measured dipole. Excluding an area of  $4^\circ$  radius around the Virgo cluster ( $l, b \approx 287^\circ, 75^\circ$ ), which is very apparent in the X-ray map, we find that it is responsible for  $\sim 20$  per cent of the total dipole, while the dipole misalignment angle with the CMB increases by  $\sim 15^\circ$ .

However, it should be expected that many Galactic sources, probably dominating the higher *ROSAT* counts, are still present in the data and could affect the behaviour of the extragalactic XRB dipole. We therefore present in figure 2 the misalignment angle between the *ROSAT* and CMB dipoles as well as the normalized dipole amplitude,  $\mathcal{D}$ , as a function of the *ROSAT* upper count limit ( $C_{up}$ ). The errorbars have been estimated by using the different Galactic model parameters resulting from the  $\chi^2$  fits of section 2.1 and presented in figure 1. We do find that our main results are very robust in such variations of the Galactic model. The two methods, used to mask the excluded regions, give consistent dipole results for  $C_{up} \lesssim 140$  (which cover  $\sim 97$  per cent of the unmasked sky). For this limit the *ROSAT* -CMB dipole misalignment angle is  $\lesssim 26^\circ$  and  $33^\circ$  for the *homogeneous filling* and *spherical harmonics* methods respectively. It is evident that the *ROSAT* -CMB dipole misalignment angle increases substantially when we include the few higher intensity cells, before however the Virgo cluster (which enters at  $C_{up} \gtrsim 200$  counts) starts reducing again the misalignment angle, as can be clearly seen in figure 2. The interpretation that the high intensity ( $C \gtrsim 140$ ) cells are associated with Galactic sources is supported by the fact that when we include these few cells the resulting dipole direction moves towards the Galactic centre. We therefore consider as our best estimate of the XRB dipole its value at  $C_{up} \approx 140$ , for which *both methods used to model the*

**Table 2.** The ROSAT Dipole Results for  $|b| > b_{lim}$ .

	mask model	$b_{lim}$	$l^\circ$	$b^\circ$	$\delta\theta_{\text{CMB}\odot}^\circ$	$\delta\theta_{\text{CMBLG}}^\circ$	$\mathcal{D}$	sky masked
raw counts	Homogeneous	20	342.7	20.4	67.6	59.5	0.050	36%
"	Sph.Harm.	20	343.0	11.0	74.5	63.8	0.092	36%
Galaxy, North Polar Spur	Homogeneous	20	280.3	29.1	21.2	3	0.011	47%
& Magellanic Clouds excluded	Sph.Harm.	20	318.3	20.1	51.1	38.5	0.037	47%
"	Homogeneous	30	290.9	41.6	19.8	16.1	0.010	63%
"	Sph.Harm.	30	313.5	14.9	51.7	36.7	0.049	63%

masked areas agree and the XRB-CMB dipole misalignment angle is minimum.

To take into account all possible sources of uncertainty, we use a Monte-Carlo simulation approach in which we vary all the model parameters within their range of validity. Using 6000 dipole realizations to take into account (a) the uncertainties of the Galactic model subtracted from the raw counts, (b) the different methods used to mask the excluded sky regions (c) the different galactic latitude limits and (d) variations of the excision radii around the bulge and the North Polar Spur we conclude that the XBG ROSAT dipole has:

$$\mathcal{D}_{\text{XRB}} \approx 0.017 \pm 0.008 \quad (l, b) \approx (286^\circ, 22^\circ) \pm 19^\circ$$

which deviates from the CMB dipole directions in the heliocentric and Local Group frames by  $\delta\theta_{\text{CMB}\odot} \sim 30^\circ$  and  $\delta\theta_{\text{CMBLG}} \sim 10^\circ$ , respectively. It is interesting that the ROSAT dipole is nearer to the Local Group frame CMB dipole direction. Our results are consistent with the HEAO-1 (2-10 keV) dipole (Shafer & Fabian 1983) which points in a similar direction ( $282^\circ, 30^\circ$ ), albeit with a larger uncertainty, but has a lower amplitude:  $\mathcal{D}_{\text{HEAO-1}} \sim 0.005$ .

### 3.3 Interpretation

The motion of the Sun with respect to an isotropic radiation background produces a dipole in the radiation intensity according to:

$$\frac{\delta\mathcal{C}}{\langle\mathcal{C}\rangle} = (3 + \alpha)V_\odot \cos\theta/c \quad (5)$$

where  $\alpha$  is the spectral index of the radiation ( $\mathcal{C} \propto \nu^{-\alpha}$ ). For the 1.5 keV ROSAT band we have  $\alpha \sim 0.4$  (Gendreau et al. 1995). If the ROSAT dipole was totally due to the motion of the Sun with respect to the XRB (Compton-Getting effect) then we would obtain a solar velocity with respect to the XRB of  $V_\odot = 1300 \pm 600$  km/sec, which should be compared with  $V_\odot = 369$  km/sec with respect to the CMB (Lineweaver et al 1996).

We therefore verify that the observed XRB ROSAT dipole cannot be only due to the Compton-Getting effect but it is significantly contaminated by the

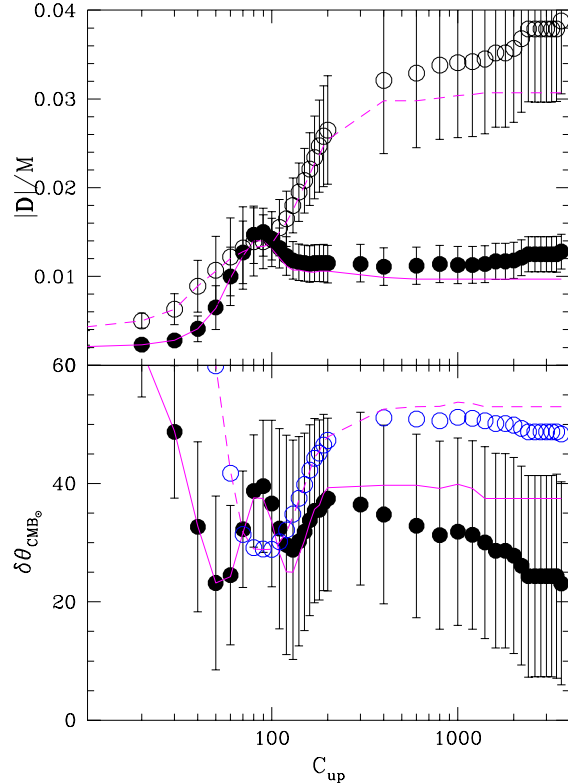


**Figure 2.** Dipole results as a function of upper count limit,  $C_{up}$ . The filled and open points correspond to the *homogeneous fill* and *Spherical harmonics* mask methods respectively. The scatter correspond to the variations of the Galaxy model, as given by all the different  $\chi^2$  fits (see section 2.1). The corresponding solutions, excluding the Virgo cluster, are shown as the continuous and dashed lines.

dipole produced by X-ray emitting sources that trace the large-scale structure. We estimate the large-scale dipole component of the XRB by subtracting from the ROSAT map the expected Compton-Getting dipole and we obtain a dipole with  $\mathcal{D}_{\text{LSS}} \approx 0.9\mathcal{D}_{\text{XRB}}$  pointing towards  $(l, b) \sim (284^\circ, 18^\circ)$ . This is in general agreement with Lahav et al (1997) who found that the two effects, contributing to the XRB dipole, are of the same order of magnitude.

#### 4 CONCLUSIONS

We have estimated the dipole of the diffuse 1.5 keV X-ray background using the *ROSAT* all-sky survey maps of Snowden et al (1995). We have first subtracted from the *ROSAT* counts the diffuse Galactic emission (the halo and bulge components) as well as local extended features such as the North Polar Spur. The Galactic halo model used is that of a finite radius disk model with an exponential scale height (eg Iwan et al 1982). The mean Galactic X-ray component is  $\sim 20 - 30$  per cent of the background and the scale height and radius are  $\sim 16 \pm 5$  and  $27 \pm 5$  kpc respectively. We model the excluded regions by either homogeneously “painting” these regions with the mean X-ray count (derived after subtracting the Galaxy) or using a spherical harmonic expansion of the X-ray surface intensity field.

We estimate that the *ROSAT* XRB dipole is pointing towards  $(l, b) \approx (286^\circ, 22^\circ) \pm 19$ , within  $\sim 30^\circ$  of the CMB direction and having a normalized amplitude of  $\sim 1.7$  per cent. The dipole direction is in agreement with previous estimates in hard X-rays (Shafer & Fabian 1982) but the positional errors have now been improved. We also find that the two effects expected to contribute to the XRB, ie., the Compton-Getting effect and the anisotropy due to X-ray sources tracing the large-scale structure, are of the same order of magnitude, in general agreement with the predictions of Lahav et al (1997). However, the latter dominates having  $D_{LSS} \sim 0.9 D_{XRB}$ . Finally we estimate that the nearest cluster, Virgo, contributes  $\sim 20$  per cent to the total measured XRB dipole.

#### ACKNOWLEDGMENTS

We thank the referee, Dr. Marie Treyer, for her helpful comments and suggestions.

#### REFERENCES

- Boldt E., 1987, Phys. Rep., 146, 215  
 Compton A., Getting I., 1935, Phys. Rev., 47, 817  
 Gendreau. K. et al. 1995, PASJ, 47, L5  
 Georgantopoulos, I., Stewart, G.C., Shanks, T., Boyle, B.J., Griffiths, R.E., 1996, MNRAS, 280, 276  
 Hasinger, G., in IAU Symposium 168, eds Kafatos M. & Kondo Y., p. 245, Kluwer  
 Hasinger, G., Burg, R., Giaconni, R., Schmidt, M., Trumper, J., Zamorani, G., 1998, AA, 329, 482  
 Iwan D., Marshall F.F., Boldt E.A., Mushotzky R.F., Shafer R.A., & Stottlemeyer A., 1982, ApJ, 260, 111  
 Jahoda K., 1993, Adv.Space Res., 13, (12)231

- Kneissl R., Egger R., Hasinger G., Soltan A.M. & Trumper J., 1997, AA, 320, 685  
 Lahav O., Edge, A.C., Fabian, A.C., Putney A., 1989, MNRAS, 238, 881  
 Lahav O., Fisher, K.B., Hoffman, Y., Schraf, C.A. & Zaroubi, S., 1994, ApJ, 423, L93  
 Lahav O., Piran T. & Treyer, M., 1997, MNRAS, 284, 499  
 Lineweaver C.H. et al, 1996, ApJ, 470, 38  
 Marshall, F.E., Boldt, E.A., Holt, S.S., Miller, R.B., Mushotzky, R.F., Rose, L.A., Rothschild, R.E., Serlemittos, P.J., 1980, ApJ, 235, 4  
 Miyaji T., Boldt E., 1990, ApJ, 353, L3  
 Nousek, J.A., Fried, P.M., Sanders, W.T., Kraushaar, W.L., 1982, ApJ, 258, 83  
 Plionis M. & Kolokotronis V., 1998, ApJ, 500, 1  
 Pietz, J., Kerp, J., Kalberla, P.M.W., Burton, W.B., Hartmann, D., Mebold, U., 1998, AA, 332, 55  
 Protheroe, R.J., Wolfendale, A.W., Wdoczyk, J., 1980, MNRAS, 192, 445  
 Shafer R.A., Fabian A.C., in Abell G.O., Chincarini G., eds, IAU Symp. No 104, Early Evolution of the Universe and its Present Structure. Kluwer, Dordrecht, p.33  
 Snowden S.L., McCammon, D., Burrows, D. N., Mendelhall, J. A., 1994, ApJ, 424, 714  
 Snowden S.L. et al, 1995, ApJ, 454, 643  
 Wang, Q.D., McCray, R., ApJ, 409, L37  
 Yahil A., Walker, D., Rowan-Robinson, M., 1986, ApJ, 301, L1